Nanoscale

Accepted Manuscript

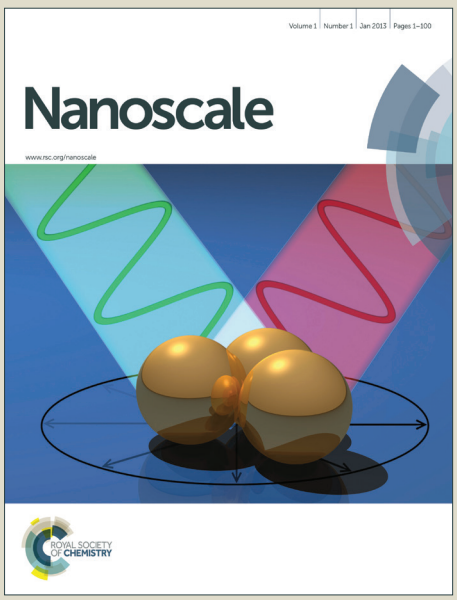

ROYAL SOCIETY OF CHEMISTRY

www.rsc.org/nanoscale

Nanoscale

RSCPublishing

ARTICLE

Composite Nanoplatelets Combining Soft-Magnetic Iron Oxide with Hard-Magnetic Barium Hexaferrite

Cite this: DOI: 10.1039/x0xx00000x

D. Primc[a]† and D. Makovec[a*]

Received 00th January 2014,
Accepted 00th January 2014

DOI: 10.1039/x0xx00000x

www.rsc.org/

By coupling two different magnetic materials inside a single composite nanoparticle, the shape of the magnetic hysteresis can be engineered to meet the requirements of specific applications. Sandwich-like composite nanoparticles composed of a hard-magnetic Ba-hexaferrite ($BaFe_{12}O_{19}$) platelet core in between two soft-magnetic spinel iron oxide maghemite (γ-Fe_2O_3) layers were synthesized using a new, simple and inexpensive method based on the co-precipitation of Fe^{3+}/Fe^{2+} ions in an aqueous suspension of hexaferrite core nanoparticles. The required close control of the supersaturation of the precipitating species was enabled by the controlled release of the Fe^{3+} ions from the nitrate complex with urea ($[Fe((H_2N)_2C=O)_6](NO_3)_3$) and by using $Mg(OH)_2$ as a solid precipitating agent. The platelet Ba-hexaferrite nanoparticles of different sizes were used as the cores. The controlled coating resulted in an exclusively heterogeneous nucleation and the topotactic growth of the spinel layers on both basal surfaces of the larger hexaferrite nanoplatelets. The direct magnetic coupling between the core and the shell resulted in a strong increase of the energy product $|BH|_{max}$. Ultrafine core nanoparticles reacted with the precipitating species and homogeneous product nanoparticles were formed, which differ in terms of structure and composition compared to any other compound in the $BaO–Fe_2O_3$ system.

Introduction

Composite nanoparticles, combining two magnetically different phases, frequently referred to as bi-magnetic nanoparticles, represent an important class of magnetic nanomaterials. An exchange bias resulting from the coupling between the ferromagnetic and antiferromagnetic phases represents an extra source of anisotropy, which increases the superparamagnetic limit - an important property limiting the miniaturization of recording media.[1] Even more important, an exchange-spring coupling between the soft-magnetic and the hard-magnetic phases combined at the nanolevel can lead to an increased energy product $|BH|_{max}$, a figure of merit for the quality of magnets.[2,3] These bi-magnetic nanoparticles are thus ideal building blocks for the preparation of exchange-spring permanent magnets with improved properties[2-5] or, alternatively, the effect of the exchange coupling can be applied to tune the properties of the nanoparticles to make them relevant for different applications. The coupling can be used to tune the shape and the temperature dependence of the nanoparticles' magnetization curve, defining properties such as the coercivity (H_C), the remanence (M_R), and the blocking temperature (T_B).[6-11]

Generally, magnetic nanoparticles can be used in a variety of technologies (e.g., in ferrofluids[12] and magnetic separation[13]) and medicine[14], where they can be used in numerous applications in vitro (e.g., the detection, separation, or sorting of specific cells, magnetofection, etc.)[15] and in vivo for diagnostics (e.g., for contrast enhancement in magnetic resonance imaging (MRI)[16] and in magnetic particle imaging (MPI)[17] and in therapy (e.g., for targeted drug delivery[18,19] and for cancer treatment using magnetically mediated hyperthermia.[7,11,20-23] Nanoparticles with an improved conversion of the electromagnetic energy into heat, which can be used as the mediators in magnetic hyperthermia and in other applications, making use of the good heating ability of the nanoparticles in an AC magnetic field,[18.20-25] are a good example of the beneficial effect of the exchange coupling in bi-magnetic nanoparticles on their relevant properties. By tuning the magnetic anisotropy of the bi-magnetic nanoparticles with coupling of the hard and the soft magnetic phases, the specific heating rate was strongly increased,[7,11,23] in some cases by almost an order of magnitude.[7] Obviously, apart from the physical properties, biological aspects are also crucial in medical applications.[14] Today, it is practically only nanoparticles of magnetic iron oxide (maghemite) that are used in biomedicine, because they are considered safe and have been approved by the US Food and Drug Ad-ministration (FDA) for in-vivo applications.[14]

To effectively tune the magnetic properties of bi-magnetic nanoparticles, the size and the shape of both the magnetic phases in intimate contact have to be carefully controlled. The effective exchange coupling of the soft phase to the hard phase requires the size of the soft phase to be less than half the domain-wall width of the hard phase.[26-29] Usually, bi-magnetic nanoparticles have a core-shell structure.[2,5-11] Nevertheless, other bi-magnetic hetero-

nanostructures were reported;[4,5,7,30] however, it was found that the exchange coupling in core/shell nanoparticles is stronger than in other composite nanostructures where the contact areas between the two materials are smaller, for example, in heterodimer nanoparticles.[5]

The core-shell architecture is also advantageous for controlling the nanoparticle structure during the synthesis. In the sequence-based synthesis route the size of the core is defined by the choice of the core nanoparticles and/or the conditions used for their synthesis in the first step, whereas the thickness of the shell is controlled in the subsequent coating process. The magnetic materials used in bi-magnetic nanoparticles include simple metals (soft-magnetic Fe and Co),[4,10,31] alloys (hard-magnetic FePt and CoPt),[2,4,5] carbides (Fe_3C, Ni_3C),[11,32] simple oxides (antiferrimagnetic FeO and MnO)[33-35], and mixed oxides. Among the mixed oxides, spinel ferrites are the most frequently exploited, with Co-ferrite ($CoFe_2O_4$) as the only hard-magnetic representative of the family, and numerous soft-magnetic representatives, including the iron oxides magnetite (Fe_3O_4) and maghemite (γ-Fe_2O_3), manganese ferrite ($MnFe_2O_4$), nickel ferrite ($NiFe_2O_4$), and zinc ferrite ($ZnFe_2O_4$, antiferrimagnetic as bulk, but soft-magnetic in the form of nanoparticles[36]).[6-9]

The method used for the synthesis of the core-shell nanoparticles may depend on the type of material; however, by far the most exploited method is the high-temperature thermal decomposition of organometallic precursors.[4-8,30] This method is based on the decomposition of organometallic compounds (e.g., metal acetylacetonate, metal-oleate complex, iron pentacarbonyl) in a high-boiling-point solvent (e.g., hexadecanediol, octadecene) and in the presence of a capping agent, oleic acid and/or oleylamine.[37,38] The method is known to be capable of producing mono-dispersed nanoparticles that are dispersible in non-polar media. The size of the nanoparticles can be closely tuned using the experimental conditions. The synthesis can be conducted in two steps (a seed-mediated particle growth method), and is therefore suitable for the synthesis of core-shell nanoparticles.[37] The drawbacks of the method are its relatively large complexity and the need for expensive, frequently toxic, starting materials. The composite nanoparticles composed of a spinel-ferrite shell at a core of a different material can also be synthesized using simple co-precipitation of metal ions in an aqueous suspension of the core nanoparticles. We report here on the first synthesis of composite nanoparticles coupling hard-magnetic properties of a Ba-hexaferrite ($BaFe_{12}O_{19}$) platelet core with soft-magnetic properties of a spinel ferrite iron oxide maghemite (γ-Fe_2O_3) shell. The maghemite shell was coated onto the hexaferrite core nanoparticles using a new, inexpensive method based on the co-precipitation of Fe^{3+}/Fe^{2+} ions in an aqueous colloidal suspension of the cores. Maghemite forms in a sequence of chemical reactions and transformations. The involved process is actually quite complex and depends significantly on the experimental conditions, e.g., reactant concentrations, the presence of counter ions, temperature, etc.;[39] however, with some simplifications we can reveal the relevant steps. Fe^{3+} precipitates to form Fe oxide hydroxide (FeOOH) already at a low pH of 2.8, whereas Fe^{2+} precipitates at a pH above 6. If the FeOOH is in its γ-FeOOH structural modification (lepidocrocite), it will react with precipitating $Fe(OH)_2$ to form magnetic spinel ferrite, first magnetite (Fe_3O_4), which usually oxidizes to maghemite (γ-Fe_2O_3) when exposed to the ambient air. Under acidic conditions with a pH below 2.8 Fe^{3+} ions can slowly precipitate due to thermal hydrolysis at elevated temperatures.[39]

Hard-magnetic Ba-hexaferrite was used for the core material. Due to its highly anisotropic, complex magnetoplumbite hexagonal structure[40] (see Fig. 1 (a)), the hexaferrite nanoparticles grow with a plate-like shape (nanoplatelets).[41,42] Besides the large magnetocrystal-line anisotropy of the hexaferrite ($K = 3.3 \cdot 10^4$ J/m^3 in the bulk),[43] the shape anisotropy of the nanoplatelets can also be exploited. For example, the first ferromagnetic liquids were prepared by dispersing hexaferrite nanoplatelets in a ferroelectric liquid crystal.[44]

Ba-hexaferrite nanoplatelets can be synthesized using the hydrothermal method.[41,42] The hydrothermal treatment of an aqueous suspension of barium and iron hydroxides in the presence of a high concentration of hydroxyl ions results in the formation of hexaferrite at relatively low temperatures.[41,42] This low formation temperature enables the synthesis of ultrafine nanoparticles. Such ultrafine nanoparticles have a discoid shape, around 10 nm wide, but only approximately 3 nm thick, which is less than 2 dimensions of the unit cell in the corresponding c-direction of their hexagonal structure. They exhibit rather poor magnetic properties, which can be ascribed to their poor structural order.[41,42,45] When the synthesis occurs at higher temperatures the nanoparticles grow with the mechanism of Ostwald ripening and larger hexagonal platelet crystals are obtained, which show hard-magnetic properties. The exaggerated growth of the nanoparticles during their hydrothermal synthesis can be suppressed with the addition of surfactants, such as oleic acid.[42]

Experimental

Materials

Iron (III) nitrate hepta hydrate ($Fe(NO)_3 \cdot H_2O$), iron (II) chloride ($FeCl_2$), barium nitrate ($Ba(NO_3)_2$), magnesium hydroxide ($Mg(OH)_2$), sodium hydroxide, (NaOH, 98%), urea, nitric (V) acid (HNO_3), citric acid (99+%), *N*,*N*-Dimethylformamide (99+%), 1,2-dichlorobenzene, and oleic acid were purchased from Alfa Aesar. All reagents were used without further purification.

Synthesis of Ba-hexaferrite core nanoparticles

Hexaferrite core nanoparticles were synthesized using the previously reported hydrothermal method[45] (the synthesis procedures are given in the Supplemental information 1). Three batches of nanoparticles, each batch with a different particle size, were used as the cores for the synthesis of the composite nanoparticles: (i) the plate-like nanoparticles $BaM_{10\text{-}70}$ represented a mixture of ultrafine discoid nanoparticles, approximately 10 nm wide and 3 nm thick, and larger nanoplatelets, up to 70 nm wide, but still just up to 5 nm thick, (ii) only ultrafine discoid nanoparticles BaM_{10} of uniform size (10 nm wide, 3 nm thick), and (iii) platelet crystals BaM_{100}, approximately 100 nm wide and 8 nm thick. (transmission electron microscopy (TEM) and high-resolution TEM (HREM) images are given in the Supplemental information 2). For the coating with the spinel-ferrite shell, the core nanoparticles were dispersed in water to form colloidally stable suspensions (details of the procedures are given in the Supplemental information 1).

Coating spinel iron oxide shell onto the core nanoparticles

The spinel iron oxide (maghemite) shell was coated on the hexaferrite core nanoparticles with the co-precipitation of the Fe^{3+}/Fe^{2+} ions in the aqueous suspension with weak hydroxide. The shell formed with heterogeneous nucleation and growth of the product at the core nanoparticles. The supersaturation of the precipitating iron species was closely controlled to enable exclusively heterogeneous nucleation by immobilizing the Fe^{3+} ions in a nitrate complex with urea $[Fe((H_2N)_2C{=}O)_6](NO_3)_3$ (later in the text: Fe^{3+}-urea complex). Thus, the release of the reacting Fe^{3+} ions can be controlled by the thermal decomposition of the complex. To homogeneously release the hydroxyl ions, a solid precipitating agent $Mg(OH)_2$ was admixed into the reaction mixture. The solubility of

$Mg(OH)_2$ is limited (0.01 g/L) and increases with the temperature.[46] The hydroxyl ions can thus be relatively homogeneously released into the reaction mixture while the pH is controlled with the temperature. Due to the immobilization into the complex, the precipitation of the Fe^{3+} is postponed to higher pH values above 6, where the Fe^{2+} is precipitated, enabling the simultaneous precipitation of the two iron ions, which was found to be crucial for avoiding unwanted side reactions.

The experimental conditions required for the deposition of the spinel ferrite layer after exclusively heterogeneous nucleation were determined in a preliminary study. If the supersaturation of the precipitating species was too high, the product partially nucleated homogeneously, and large, octahedrally-shaped spinel-ferrite nanoparticles were formed in addition to the composite nanoparticles (see the TEM image in the Supplemental information 3).

The optimized process was as follows: Fifty mL of the stable aqueous suspension containing the core nanoparticles was heated to 60 °C under argon bubbling. The amount of core nanoparticles was determined from their estimated surface area of 5.45 m^2, which would result in a calculated thickness of the shell after the reaction of approximately 3 nm. The Fe^{3+}-urea complex (0.12 mmol) and $FeCl_2$ (0.06 mmol) were dissolved in the suspension (pH=2.2) and mixed for 15 minutes. At this elevated temperature the Fe^{3+}-urea complex slowly decomposes and the released Fe^{3+} ions hydrolyze to form the γ-FeOOH product. After the time allowed for the thermal hydrolysis, the $Mg(OH)_2$ was admixed into the reaction mixture. The slow increase to a pH of 6.8 resulted in an almost simultaneous precipitation of Fe^{2+} and the remaining Fe^{3+} released from the complex, resulting in the transformation of the γ-FeOOH into the magnetic spinel ferrite product and its subsequent growth. After 2 hours at the final pH the reaction mixture was cooled to room temperature. The entire procedure was conducted under an inert atmosphere of argon.

Characterizations

The nanoparticles were characterized using transmission electron microscopy (TEM) in combination with energy-dispersive X-ray spectroscopy (EDXS). For the TEM analysis, the nanoparticles were suspended in ethanol and deposited on a copper-grid-supported perforated electron-transparent carbon foil. A field-emission electron-source TEM JEOL 2010F equipped with an Oxford Instruments ISIS300 EDXS detector was operated at 200 kV. Quantitative EDXS analyses were performed using Oxford ISIS software. The spectrum taken from the largest Ba-hexaferrite core nanoparticles of the sample BaM_{100} was used as a standard during the quantization of the spectra collected from the other nanoparticles. The relative error of the analysis, tested on the nanoparticles $BaM_{100,}$ was estimated to be less than ± 7 % for Fe and less than ± 15 % for Ba. The X-ray diffractometry (XRD) of the nanoparticles was performed using a PANalytical X` Pert PRO diffractometer. The magnetic properties of the samples were measured at room temperature using a Lake Shore 7312 vibrating-sample magnetometer. To avoid the problem of an unknown orientation, the largest nanoparticles BaM_{100} and $S@BaM_{100}$ were measured after they were magnetically oriented. The nanoparticles were first hydrophobized by the adsorption of oleic acid onto their surfaces and then a low concentration of nanoparticles was homogeneously dispersed in a liquid wax heated to 80 ^oC. After magnetic orientation in a homogeneous magnetic field of 1 T the wax was solidified by cooling.

Results and discussion

Structure of composite nanoparticles

The structure of the nanoparticles that were synthesized by coating the hexaferrite core nanoparticles with the spinel-ferrite layer was revealed by the (HR)TEM imaging. To observe the structure, the platelet nanoparticles have to be oriented edge on, i.e., with the large surfaces parallel to the electron beam. Due to the platelet shape, the nanoparticles tend to lie flat on the specimen support. To maximize the number of nanoparticles oriented edge on, they were deposited onto the TEM specimen support in an agglomerated state. Between 150 and 300 nanoparticles, oriented edge on, were analyzed for each sample in order to provide a statistically significant result.

Coating the BaM_{10-70} cores with a bimodal size distribution (the $S@BaM_{10-70}$ sample) resulted in the synthesis of two different types of Ba and Fe-containing nanoparticles: larger composite nanoparticles and smaller uniform nanoparticles. Separate nanoparticles of spinel ferrite or particles with any other phases were never detected in the sample. The larger composite nanoparticles showed a typical "sandwich"-type structure. The TEM image (Fig. 1(b)) of the platelet nanoparticles oriented edge on clearly shows that the nanoparticles are composed of a hexaferrite core in between two layers of different material. The layers were homogeneous and with a uniform thickness. The layer thickness was measured for more than 70 composite nanoparticles, oriented edge on, to be 2.1±0.5 nm. The analysis of the HREM images (Fig. 1(c)) clearly showed the spinel structure of the single-crystalline layers, whereas the EDXS analysis showed the presence of only Fe and O. During co-precipitation of the Fe^{3+}/Fe^{2+} ions from the aqueous solution under an inert atmosphere magnetite is formed as the spinel ferrite product; however, it is most probably completely oxidized into maghemite when exposed to the ambient air.[39] The two structures, i.e., the magnetoplumbite structure of the hexaferrite core and the spinel structure of the layers, are related. The magnetoplumbite structure can be represented as a hexagonal stacking of close-packed layers composed of larger oxygen and barium ions with smaller iron ions at the interstitial positions. The structure can be divided into alternating structural blocks: the Ba-containing R block with hexagonal stacking and the S block with cubic stacking, which represents a (111) slice of the common spinel structure[40] (Fig. 1(a)). The HREM image (Fig. 1(c)) of the hexaferrite core is characterized by a dominant periodicity of 1.15 nm, corresponding to the $(0002)_{HF}$ interplanar distances of its hexagonal structure. The spinel layers grow topotactically on both the basal-plane surfaces of the hexaferrite core platelet with close-packed (111) planes of its cubic structure parallel to the basal planes of the hexaferrite. Thus, a coherent interface is formed, since both the structures at those planes match closely. The spinel was never situated at the side surfaces of the hexaferrite platelets, where there is no matching between the two structures.

The EDXS analysis of a large number of the individual sandwich composite nanoparticles showed that they contained 1.8±0.5 at.% Ba and 38.5±0.5 at.% Fe.

In the same sample $S@BaM_{10-70}$, the smallest nanoparticles did not show the sandwich structure exhibited by the larger ones. They maintained the homogeneous structure as the ultrafine cores, but grew somewhat thicker after the coating. The EDXS analysis showed that they contained a higher content of Ba compared to the larger, sandwich composite nanoparticles. This puzzle was solved by analyzing the nanoparticles obtained by coating only the ultrafine core nanoparticles BaM_{10}. It appeared that the smallest core nanoparticles chemically reacted during the coating procedure to form homogeneous product nanoparticles. The product nanoparticles (Fig. 1(e)) are much thicker (~9 nm) than the ultrafine cores (3 nm) (Fig. 1(d)). A HREM image (Fig. 1(e)) shows a uniform periodicity

along the thickness of the product nanoparticle; however, with the dominant periodicity being significantly smaller (0.95 nm) than that of the hexaferrite (1.15 nm). Moreover, the EDXS analysis showed that they contain 2.2±0.3 at.% Ba and 37.9 ± 0.2 at % of Fe. Thus, especially the content of Ba is a significantly lower than in the stoichiometric Ba-hexaferrite (3.125 at.%). During heating at 600 °C those product nanoparticles decomposed into the two thermodynamically-stable compounds as they grew: hexaferrite and spinel ferrite. In conclusion we can say that those product nanoparticles are different in terms of composition and structure with respect to any known compound from the Ba-Fe-O system.[47] They can be treated as the new compound, but one that is only (meta)stable when at the nano size.

When the spinel was coated onto the largest core platelets BaM_{100}, the layers formed after nucleation at several points on the cores' basal surfaces resulted in an increased roughness of the layers (Fig. 2). However, the spinel still grew topotactically on the hexaferrite, as visible in the HREM image and the corresponding electron diffraction pattern of the composite platelet oriented edge-on (Fig. 2(c)). The diffraction pattern is a superimposition of the pattern coming from the hexaferrite oriented along $[0001]_{HF}$ and the pattern from the spinel ferrite layers, oriented along the $[110]_S$ projection. Separate particles containing no Ba were never found in any of the samples after coating, proving that all the material precipitated in the coating process nucleated heterogeneously and grew at the surfaces of the larger core nanoparticles or it reacted with the ultrafine cores.

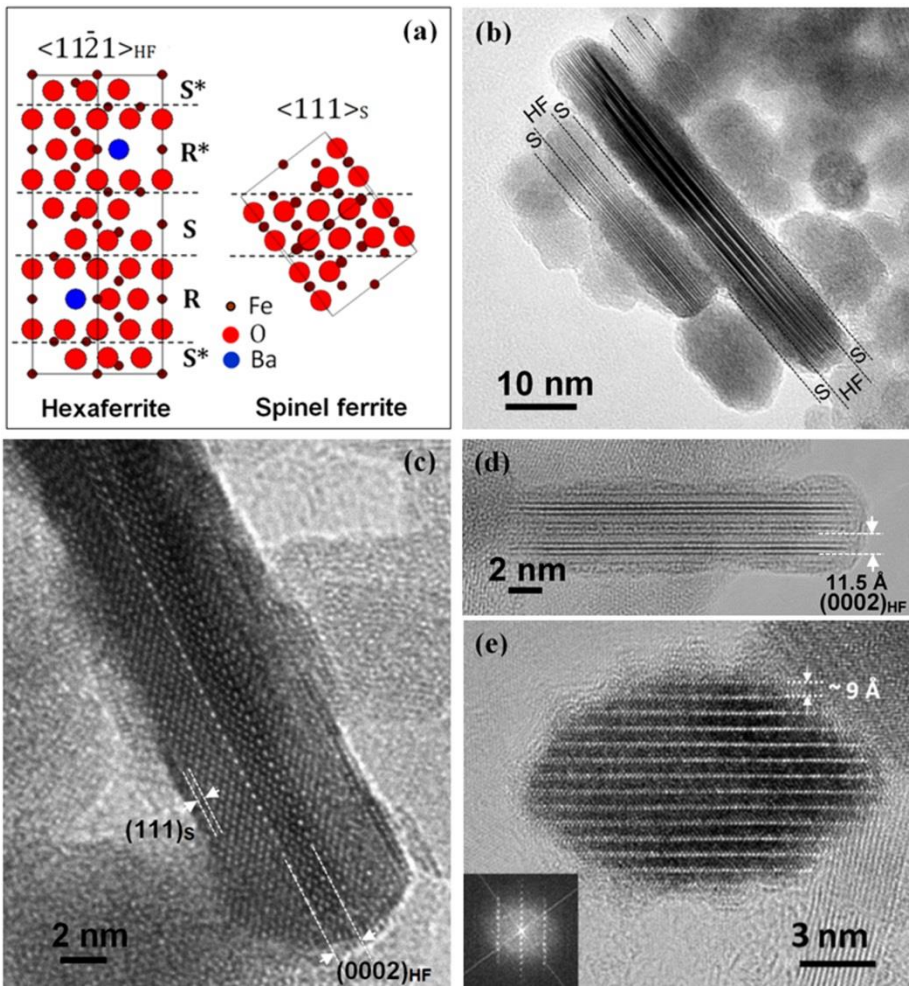

Fig. 1 (a) Schematic presentation of hexaferrite (HF) and spinel ferrite (S) structure, (b) TEM image of the of the platelet composite nanoparticles oriented edge on, with large surfaces parallel to the electron beam (sample $S@BaM_{10\text{-}70}$), (c) HREM image of the platelet composite nanoparticle ($Z = <1010>_{HF} \parallel <110>_S$) (sample $S@BaM_{10\text{-}70}$), (d) HREM image of the BaM_{10} nanoparticles before and (e) after coating with the spinel (inset: fast Fourier transform (FTT) of the HREM image).

Fig. 3 shows the XRD spectra of the core and the composite nanoparticles. The core nanoparticles show the characteristic XRD spectra, strongly influenced by their small size and the platelet shape.[41,42,45] The positions of all the peaks in the XRD spectra correspond to the hexaferrite $BaFe_{12}O_{19}$ structure; however, the intensities of the peaks differ significantly compared to those of the standard. Because of the very small dimensions of the crystal along the c-direction of the structure, which corresponds to the thickness of the nanoparticles, the (hkℓ) peaks are very broad or even missing for $\ell \neq 0$. After the coating with the spinel ferrite, additional peaks appear in the spectra of the composite nanoparticles. The positions of a majority of these peaks correspond to the spinel structure. In the spectra of the composite nanoparticles $S@BaM_{10}$ and $S@BaM_{10\text{-}70}$,

which contained product nanoparticles resulting from the chemical reaction between the core and the "shell", an additional peak is observed at $2\theta = 28.44^{0}$. In the spectrum of S@BaM_{100} the peaks of the spinel phase were hardly resolved because of the partial overlapping with the peaks of the hexaferrite and the preferential orientation of the platelet nanoparticles.

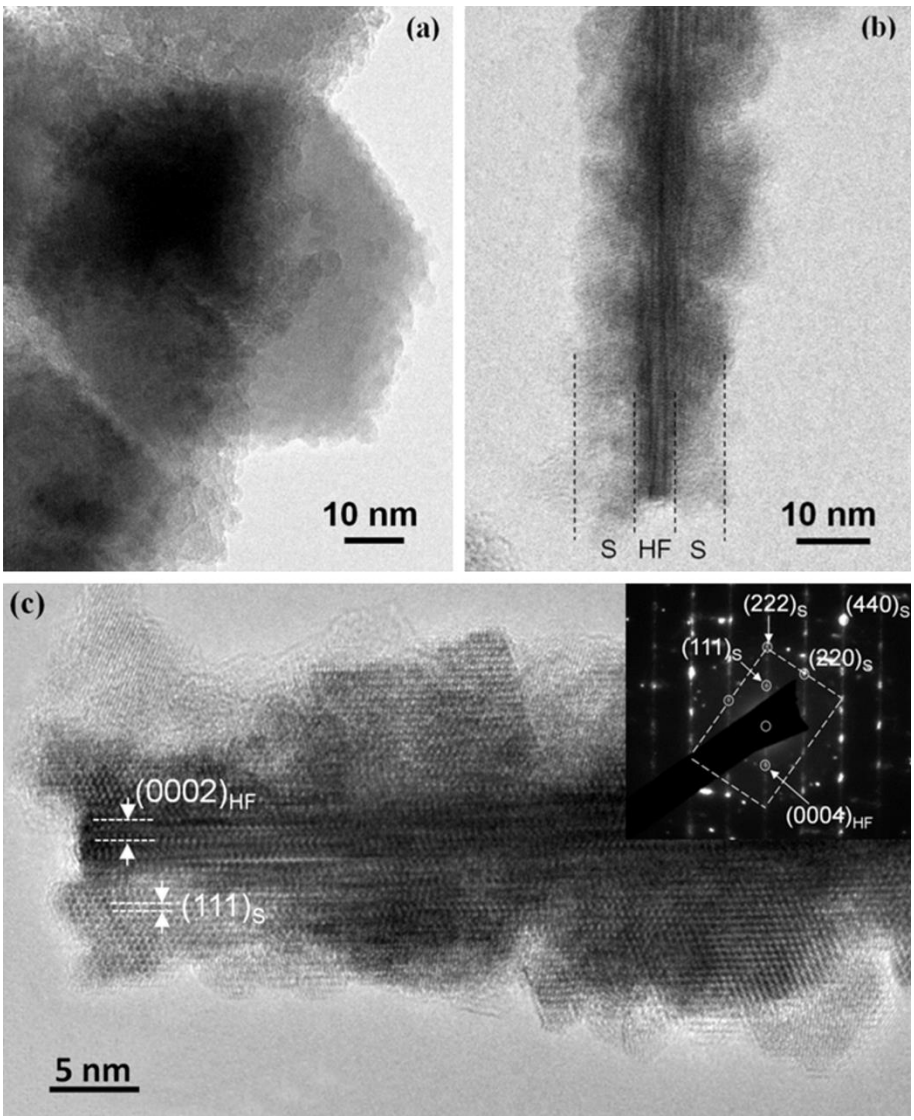

Fig. 2 TEM images of the composite nanoparticles S@BaM_{100} lying flat on the specimen support (a) and oriented edge-on (b); and HREM image (c) with a corresponding electron diffraction pattern ($[-1010]_{HF} \parallel [001]_S$, S… spinel, HF…hexaferrite).

Magnetic properties

The comparison between the magnetic hystereses of the $BaM_{10\text{-}70}$ core nanoparticles and the corresponding bi-magnetic nanoparticles S@$BaM_{10\text{-}70}$ (Fig. 4(a)) showed a strongly increased saturation magnetization (M_S) and remanence (M_R), and a somewhat decreased coercivity (H_C) of the nanocomposites (Table 1), in agreement with the presence of the soft-magnetic spinel. The magnetization is also affected by the presence of the product nanoparticles, i.e., the ultrafine nanoparticles, which reacted with the "shell". The product nanoparticles S@BaM_{10} showed weak ferrimagnetism (Fig. 4(b)); however, their magnetization at high field strengths was low (Table 1).

The largest composite nanoparticles S@BaM_{100} showed particularly interesting magnetic properties (Fig. 4 (c)). They showed a much larger M_S and M_R than the BaM_{100} core nanoparticles and a somewhat smaller H_C (Table 1). Although the composite nanoparticles were composed of the two magnetically-different phases, they displayed a single-phase magnetic loop similar to a conventional permanent magnet, proving that the two phases are exchanged coupled.[2,48] The presence of any significant amount of the non-coupled, soft-magnetic spinel ferrite in the hard-magnetic hexaferrite would lead to a characteristic constricted shape for the hysteresis loop. As an illustration, a hysteresis loop from a physical mixture of the BaM_{100} core nanoparticles and the octahedrally shaped maghemite nanoparticles S (approximately 25 nm in size, see Fig. S4(b) in the Supplemental information 4) is also shown in Fig. 4(c). The maghemite nanoparticles S had a comparable volume to the soft-magnetic layer at the hexaferrite core of the S@BaM_{100} composite nanoparticles and, therefore. presumably had comparable magnetic properties. They were mixed with the BaM_{100} nanoparticles in the S/BaM_{100} weight ratio corresponding to the estimated phase composition of the S@BaM_{100} composite

nanoparticles. This phase composition was estimated from the Ba/Fe ratio (measured using ICP-AS of the dissolved nanocomposite) to be 61.5 wt.% of $BaFe_{12}O_{19}$ / 38.5 wt.% of Fe_2O_3. Because of the rare direct contacts between the two phases in the mixture there was no direct magnetic coupling and the shape of the hysteresis is completely different to that of the bi-magnetic composite nanoparticles (Fig. 4(c)). The small difference in the M_S of the mixture and the nanocomposite reflects the error in the estimation of the phase composition and the differences in the magnetic properties of the spinel-ferrite phase in the two samples.

The shape of the mixture's hysteresis loop is already significantly changed when a small amount (2 wt.%) of the non-coupled, soft-magnetic spinel ferrite is admixed with the hard-magnetic hexaferrite (measured and calculated hysteresis loops of the physical mixtures are given in the Supplemental information 4).

The magnetic properties of the samples can also be influenced by the preferential orientation of the plate-like nanoparticles in the powder. To avoid the problem of an unknown orientation, the largest core nanoparticles BaM_{100} and the corresponding composite nanoparticles $S@BaM_{100}$ were measured after they were magnetically oriented. The large difference between the in-plane and the out-of-plane hystereses (Fig. 4(d)) suggests very good magnetic orientation of the nanoparticles (Table 1). The comparison between the in-plane hystereses of the core and the composite shows a large increase in M_S and M_R for the nanocomposite, while the decrease in H_C was small (Table 1). As a result, the energy product $|BH|_{max}$ was strongly increased in the composite, by a factor of more than two (BaM_{100}: $|BH|_{max}$ =7.2 kJ/m^3; $S@BaM_{100}$: $|BH|_{max}$ =15.2 kJ/m^3). The increase in $|BH|_{max}$ is obviously a consequence of the direct magnetic exchange-spring coupling between the hard-magnetic hexaferrite core and the soft-magnetic spinel layers.

Table 1 Magnetic properties of the samples: saturation magnetization M_S (or magnetization measured at a high field strength of 800 kA/m for the ultrafine nanoparticles), remanence M_R, and coercivity H_C (|| … in-plane measurement of the magnetically-oriented nanoparticles BaM_{100} and $S@BaM_{100}$).

Sample	M_S [Am^2/kg]	M_R [Am^2/kg]	H_C [kA/m]
$BaM_{10\text{-}70}$	7.1	2.6	31
$S@BaM_{10\text{-}70}$	31.6	2.2	12
BaM_{10}	1.5	0.05	4
$S@BaM_{10}$	3.4	0.03	<0.01
BaM_{100}	34.5	18.3	239
$S@BaM_{100}$	56.9	28.5	179
BaM_{100} ||	34.5	31.4	243
$S@BaM_{100}$ ||	56.9	48.9	192

The synthesis of new, bi-magnetic nanoparticles, combining a hard-magnetic platelet, Ba-hexaferrite core and a soft-magnetic spinel ferrite, maghemite shell, could be of major scientific and technological importance. By coupling the properties of the two magnetic materials, the shape of the hysteresis can be tailored. In a single magnetic material the shape of the magnetic hysteresis loop depends on its intrinsic magnetic properties, i.e., saturation magnetization M_S and magnetocrystalline anisotropy K_1, and extrinsic properties related to the size and the shape of the particles. Generally, hard-magnetic materials, such as hexaferrites, show a high K_1, which makes it possible to achieve a high coercivity H_C, while their M_S is limited and cannot be greatly improved, for example, by chemical substitutions of the constituting ions in their structure.[49] On the other hand, soft magnetic materials like maghemite generally display a low H_C, but a relatively high M_S. This means that in practice it is impossible to combine a high H_C and a high M_S inside a single-component magnetic material. In nanoparticles, the magnetic properties are further decreased with the decreasing size. The M_S in nanoparticles decreases due to the large proportion of "magnetically dead" surface atoms, whereas the H_C first increases with the decreasing size of the magnetic particles, reaching a maximum at the transition from a multi-domain to a single-domain state (at a particle size of few hundreds of nm for hexaferrites),[50] but decreases for even smaller particles, to reach zero at the transition to a superparamagnetic state (below 10 nm for hexaferrite). In the fine nanoparticles the magnetic properties are additionally impaired by the adaptation of their crystalline structure to the small size. This effect is especially pronounced in nanoparticles of mixed oxides with a complex structure, such as hexaferrites.[45] Thus, there are practically no possibilities to strongly improve the basic magnetic properties of the single-component nanoparticles.

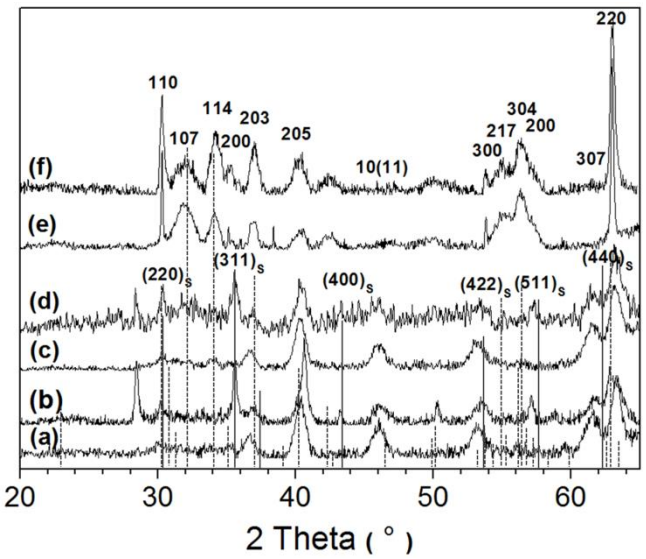

Fig. 3 XRD spectra of the core nanoparticles BaM_{10} (spectrum (a)), $BaM_{10\text{-}70}$ (c) BaM_{100} (e) and the composite nanoparticles $S@BaM_{10}$ (b), $S@BaM_{10\text{-}70}$ (d), and $S@BaM_{100}$ (f). The peaks of Ba-hexaferrite are marked with dashed lines and indexed above the spectra, while the peaks corresponding to spinel ferrite are marked with full lines and indexed by $(hk\ell)_S$.

In our work we demonstrated a simple, aqueous-based procedure that enables the synthesis of composite nanoparticles combining the relatively large H_C of the hexaferrite core with the large M_S of the maghemite shell. The topotactic growth of the spinel shell on the hexaferrite core supported the direct magnetic coupling between the core and the shell, resulting in the increased remanence M_R of the composite nanoparticles. Such bi-magnetic nanoparticles can be, for example, applied in high-density storage media. Nanoparticles with an adapted hysteresis loop shape can also be important for applications in medicine. For example, Veverka et al.[23] proposed the use of composite nanoparticles, coupling spinel ferrite and hexaferrite, as mediators in a cancer treatment based on magnetic hyperthermia. It is advantageous that the new composite nanoparticles consist almost entirely of iron oxide, which is already a standard material for medical applications involving

nanoparticles.[14] The low content of barium can be substituted with non-toxic strontium. The core $SrFe_{12}O_{19}$ nanoparticles can be synthesized using a similar hydrothermal method to that used for $BaFe_{12}O_{19}$ nanoparticles.[51]

The improved M_R and M_S of the bi-magnetic nanoparticle resulted in a large increase of the energy product $|BH|_{max}$, a figure of merit for the quality of permanent magnets. The $|BH|_{max}$ of the composite nanoparticles was doubled compared to that of the hexaferrite cores. The hexaferrites show the largest $|BH|_{max}$ of all oxide materials, and are by far the most important magnetic materials in terms of production quantities for permanent-magnet applications, mainly because of their low price.[52] Their problem is in the relatively low M_R and M_S, which were strongly improved in the bi-magnetic nanoparticles. The bi-magnetic nanoparticles can thus be applied as building blocks for the preparation of inexpensive permanent magnets with improved, anisotropic magnetic properties, high electric resistivity and excellent chemical stability. The hexaferrite core of the bi-magnetic platelets displays a strong uniaxial magnetocrystalline anisotropy, perpendicular to the basal plane of the platelet, corresponding to the crystallographic c-axis, which in combination with a large shape anisotropy enables the orientation of the nanoparticles with an applied magnetic field. Alternatively, the composite nanoparticles can be simply aligned, due to their platelet shape, during deposition from the suspension.[53] For example, magnetically oriented films can be prepared by the deposition of nanoparticles from suspensions under an electric or magnetic field and applied in self-biased nonreciprocal devices.[54]

The strong magnetic and shape anisotropy displayed by the new composite nanoparticles can also be of great importance in some other applications, for example, in the preparation of multiferroic liquids by dispersing magnetic nanoplatelets in a ferroelectric liquid crystal.[44] Up to now, only isotropic bi-magnetic oxide nanoparticles with cobalt ferrite ($CoFe_2O_4$) as the hard-magnetic phase were synthesized.[6-8] As the $CoFe_2O_4$ displays a cubic magnetocrystalline anisotropy with the easy axis along either of the <111> directions, such isotropic nanoparticles cannot be magnetically aligned.

The $|BH|_{max}$ of the bi-magnetic nanoparticles remains low when compared to that of alloys such as Nd-Fe-B, Sm-Co, or Fe-Pt; however, the new nanocomposite material does not contain any expensive noble metals or rare earths and is therefore much cheaper. A poor chemical stability and a large electrical conductivity also strongly limit the applicability of metallic magnets. This is particularly important at high frequencies, where metallic magnets cannot be used.

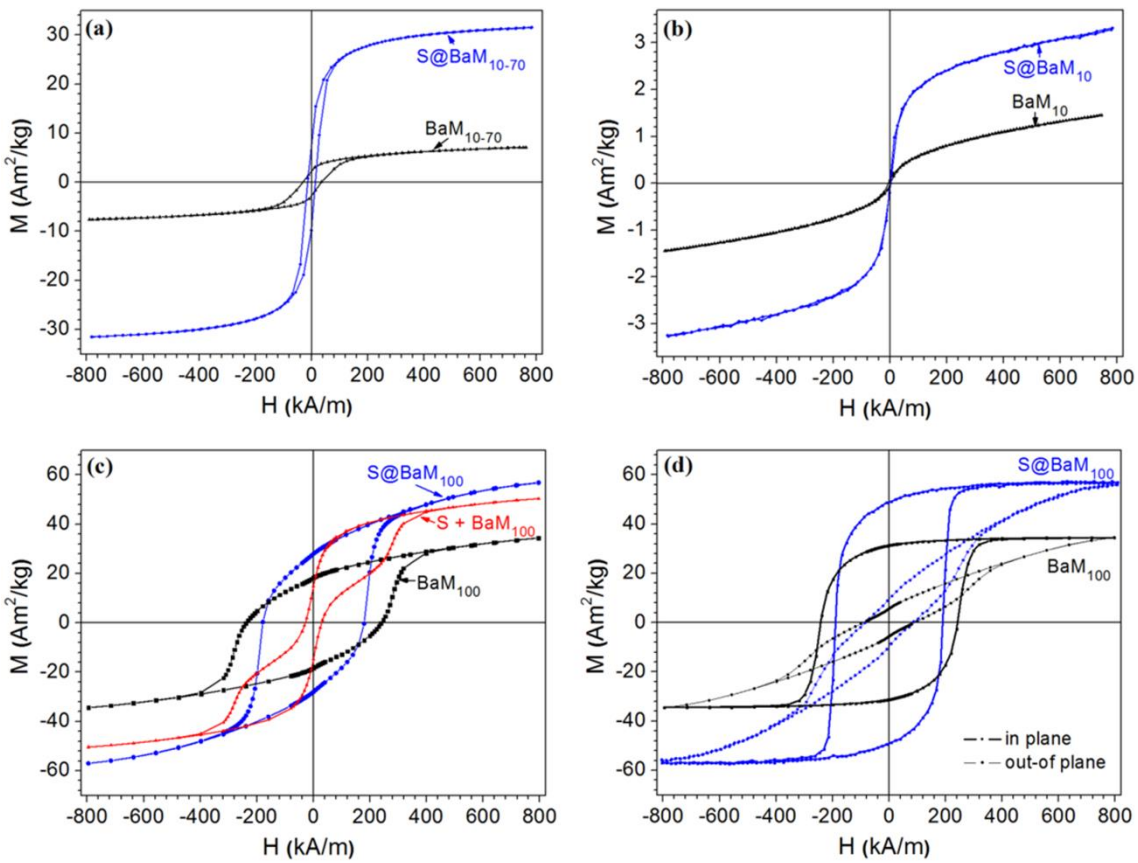

Fig. 4 Comparison of the magnetic hystereses: (a) BaM_{10-70} core nanoparticles and $S@BaM_{10-70}$ bi-magnetic composite nanoparticles, (b) BaM_{10} nanoparticles before and after coating ($S@BaM_{10}$), (c) BaM_{100} cores, $S@BaM_{100}$ nanocomposites, and the physical mixture of the BaM_{100} cores and the maghemite nanoparticles ($S + BaM_{100}$), and (d) in-plane and out-of-plane measurements of magnetically oriented BaM_{100} core nanoparticles and $S@BaM_{100}$ nanocomposites.

Conclusions

We have demonstrated the synthesis of bi-magnetic, sandwich-type, composite nanoparticles, coupling the hard-magnetic properties of the hexaferrite platelet core with the soft-magnetic properties of spinel ferrite layers for the first time, using a new, simple and inexpensive method in the aqueous suspensions. The method is based on the deposition of thin layers of iron oxide maghemite with the co-precipitation of Fe^{3+}/Fe^{2+} ions in a colloidal aqueous suspension of core nanoparticles. When the larger hexaferrite nanoplatelets (more than approximately 20 nm wide and more than 4 nm thick) are coated, the sandwich-type composite nanoparticles are formed. The spinel ferrite layers only grow topotactically at the basal-plane surfaces of the hexaferrite core, where the magnetoplumbite structure of the hexaferrite and the spinel structure of the spinel iron oxide match closely, while the spinel is never present at the side surfaces of the platelets. Thus, the composite nanoparticle display a "sandwich"-type structure. Direct, exchange-spring magnetic coupling between the hard-magnetic core and the soft-magnetic shell results in a strong increase of the energy product $|BH|_{max}$, by more than two times that of the core. Such inexpensive composite nanoparticles with excellent and highly anisotropic magnetic properties, high resistivity, and chemical stability could be very important in a variety of applications, such as high-density storage media or in medicine, for example, as mediators for magnetic hyperthermia, or they can be used as the building blocks for inexpensive permanent magnets. When the ultrafine core nanoparticles, only 10 nm wide and 3 nm thick, were coated they reacted with the precipitating species and homogeneous product nanoparticles were formed, which differ in terms of structure and composition compared to any other compound in the $BaO–Fe_2O_3$ system.

Acknowledgements

The support of the Ministry of Higher Education, Science and Technology of the Republic of Slovenia is gratefully acknowledged. The authors also acknowledge the use of equipment in the Center of Excellence on Nanoscience and Nanotechnology – Nanocenter.

Notes and references

[a] *Department for Materials Synthesis, Jožef Stefan Institute and Jožef Stefan International Postgraduate School, Jamova cesta 39, SI-1000 Ljubljana, Slovenia*

† Current address: ETH Zürich, Laboratory for Multifunction-al Materials Department of Materials, Vladimir-Prelog-Weg 5, 8093 Zurich, Switzerland

Electronic Supplementary Information (ESI) available: Synthesis (Supporting Information #1) and properties (Supporting Information #2) of the barium hexaferrite core nanoparticles, TEM of the nanoparticles synthesized under an excessive supersaturation (Supporting Information #3), and magnetic properties of physical mixtures of the hard-magnetic hexaferrite and the soft-magnetic spinel ferrite (Supporting Information #4). See DOI: 10.1039/b000000x/

1 V. Skumryev, S. Stoyanov, Y. Zhang, G. Hadjipanayis, D. Givord and J. Nogues, *Nature* 2003, **423**, 850−853.

2 H. Zeng, J. Li, J. P. Liu, L. Z. Wang and S. Sun, *Nature* 2002, **420**, 395−398.

3 D. J. Sellmyer, *Nature* 2002, **420**, 374−375.

4 Y. Yu, K. Sun, Y. Tian, X.-Z. Li, M. J. Kramer, D. J. Sellmyer, J. E. Shield and S. Sun, *Nano Lett.* 2013, **13**, 4975−4979.

5 V. Nandwana, G. S. Chaubey, K. Yano, C.-B. Rong and P. Liu, *J. Appl. Phys.* 2009, **105**, 014303-1−014303-5.

6 Q. Song and Z. J. Zhang, J. Am. Chem. Soc. 2012, **134**, 10182−10190.

7 J.-H. Lee, J.-T. Jang, J.-S. Choi, S.-H. Moon, S.-H. Noh, J.-W. Kim, J.-G. Kim, I.-S. Kim, K.-I. Park and J. Cheon, *Nature Nanotechnol.* 2011, **6**, 418−422.

8 O. Masala, D. Hoffman, N. Sundaram, K. Page, T. Proffen, G. Lawes and R. Seshadri, *Solid State Sci.* 2006, **8**, 1015−1022.

9 L. Wang, X. Wang, J. Luo, B. N. Wanjala, C. Wang, N. A Chernova, M. H. Engelhard, Y. Liu, I.-T. Bae and C.-J. Zhong, *J. Am. Chem. Soc.* 2010, **132**, 17686−17689.

10 J.-Y. Bigot, H. Kesserwan, V. Halté, O. Ersen, M. S. Moldovan, T. H. Kim, J.-T. Jang and J. Cheon, *Nano Lett.* 2012, **12**, 1189−1197.

11 A. Meffre, B. Mehdaoui, V. Kelsen, P. F. Fazzini and J. Carrey, *Nano Lett.* 2012, **12**, 4722−4728.

12 A. Blums, M. Cebers and M. Maiorov, *Magnetic Fluids*; Walter de Gruyter & Co.: Berlin, 1996.

13 L. Borlido, A. M. Azevedo, A. C. A. Roque and M. R. Aires-Barros, *Biotech. Adv.* 2013, **31**, 1374–1385.

14 *Magnetic Nanoparticles: From Fabrication to Clinical Applications*, T. K. N. Thanh, , Ed.; CRC Press: Boca Raton, USA, 2012.

15 I. Safarik and M. Safarikova In *Magnetic Nanoparticles: From Fabrication to Clinical Applications*; N. T. K. Thanh, Ed.; CRC Press: Boca Raton, USA, 2012, pp. 215-241.

16 R. Weissleder, M. Nahrendorf and M. J. Pittet, *Nature Mater.* 2014, **13**, 125−138.

17 B. Gleich and J. Weizenecker, Nature 2005, **435**, 1214−1217.

18 B. P. Timko, K. Whitehead, W. Gao, D. S. Kohane, O. Farokhzad, D. Anderson and R. Langer *Ann. Rev. Mater. Res.* 2011, **41**, 3.1–3.20.

19 M. K. Yu, Y. Y. Jeong, J. Park, S. Park, J. W. Kim, J. J. Min, K. Kim and S. Jon, *Angew. Chem. Int. Ed.* 2008, **47**, 5362−5365.

20 B. Thiesen and A. Jordan, *Int. J. Hyperthermia* 2008, **24**, 467–474.

21 E. Pollert and K. Závêta In *Magnetic Nanoparticles: From Fabrication to Clinical Applications*; N. T. K. Thanh, Ed.; CRC Press: Boca Raton, USA, 2012, pp. 449−478.

22 P. Cherukuri, E. S. Glazer and S. A. Curley, *Adv. Drug. Deliv. Rev.* 2010, **62**, 339–345.

23 P. Veverka, E. Pollert, K. Závêta, S. Vasseur and E. Duguet, *Nanotehnology* 2008, **19**, 215705-1−215705-7.

24 T. Y. Liu, S. H. Hu, D. M. Liu, S. Y. Chen and I. W. Chen, *Nano Today* 2009, **4**, 52–65.

25 H. Huang, S. Delikanli, H. Zeng, D. M. Ferkey and A. Pralle, *Nature Nanotech.* **2010**, *5*, 602–606.

26 T. Teranishi, Y. Inoue, M. Nakaya, Y. Oumi and T. Sano, *J. Am. Chem. Soc.* 2004, **126**, 9915−9916.

27 Y. L. Hou, H. Kondoh, T. Kogure and T. Ohta, *Chem. Mater.* 2004, **16**, 5149−5152.

28 T. Teranishi, M. Saruyama, M. Nakaya and M. Kanehara, *Angew. Chem., Int. Ed.* 2007, **46**, 1713−1715.

29 Y. L. Hou, Z. C. Xu, S. Peng, C. B. Rong, J. P. Liu and S. H. Sun, *Adv. Mater*. 2007, **19**, 3349−3352.

30 M. Casavola, A. Falqui, M. A. Garcia, M. Garcia-Hernandez, C. Giannini, R. Cingolani and P. D. Cozzoli, *Nano Lett.* 2009, **9**, 366−376.
31 C. Binns, M. T. Qureshi, D. Peddis, S. H. Baker, P. B. Howes, A. Boatwright, S. A. Cavill, S. S. Dhesi, L. Lari, R. Kroeger and S. Langridge, *Nano Lett.* 2013, **13**, 3334−3339.
32 W. Zhou, K. Zheng, L. He, R. Wang, L. Guo, C. Chen, X. Han and Z. Zhang, *Nano Lett.* 2008, **8**, 1147−1152.
33 S. Kang, G. X. Miao, S. Shi, Z. Jia, D. E. Nikles and J. W. Harrell, *J. Am. Chem. Soc*. 2006, **128**, 1042−1043.
34 G. Salazar-Alvarez, H. Lidbaum, A. Lopez-Ortega, M. Estrader, K. Leifer, J. Sort, S. Surinach, M. D. Baro and J. Nogues, *J. Am. Chem. Soc*. 2011, **133**, 16738–16741.
35 X. Sun, N. Frey Huls, A. Sigdel and S. Sun, *Nano Lett.* 2012, **12**, 246−251.
36 T. Sato, K. Haneda, M. Seki and T. Iijima, *Appl. Phys.* 1990, **A50**, 13−16.
37 S. H. Sun, H. Zeng, D. B. Robinson, S. Raoux, P. M. Rice, S. X. Wang and G. Li, *J. Am. Chem. Soc*. 2004, **126**, 273–279.
38 J. Park, K. An, Y. Hwang, J.-G. Park, H.-J. Noh, J.-Y. Kim, J.-H. Park, N.-M. Hwang and T. Hyeon, *Nature Materials* 2004, **3**, 891−895.
39 R.M. Cornell and U. Schwertmann, *The Iron Oxides; Structure, Properties, Reactions, Occurrences and Uses*, Wiley-VCH: Weinheim, 2003.
40 E. Pollert, *Prog. Cryst. Growth. Charact*. 1985, **11**, 155−205.
41 M. Drofenik, I. Ban, G. Ferk, D. Makovec, A. Žnidaršič, Z. Jagličič and D. Lisjak, *J. Am. Ceram. Soc.* 2010, **93**, 1602−1607.
42 D. Primc, D. Lisjak, D. Makovec and M. Drofenik, N*anotechnology* 2009, **20**, 315605-1−315605-9.
43 J. Smith and H. P. J. Wijn, *Ferrites*; Philips Technical Library: Eindhoven, 1962.
44 A. Mertelj, D. Lisjak, M. Drofenik and M. Čopič, *Nature* 2013, **504**, 237−241.
45 D. Makovec, D. Primc, S. Šturm, A. Kodre, D. Hanžel and M. Drofenik, *J. Sol. State Chem.* 2012, **196**, 63−71.
46 N. N. Greenwood and A. Earnshaw, *Chemistry of Elements*, Elsevier Butterworth-Heinemann: Oxford, 2006.
47 H. J. van Hook, *J. Am. Ceram. Soc.*, 1964, **47**, 579-581.
48 E. F. Kneller and R. Hawig, *IEEE Trans. Mag.* 1991, **27**, 3588-3600.
49 H. Taguchi, T. Takeishi, K. Suwa, K. Masuzawa and Y. Minachi, *J. Phys. IV (France)* 1997, **7,** C1-311−C1-312.
50 E. C. Stoner and E. P. Wohlfarth, *Phil. Trans. R. Soc. (London), Ser. A*, 1948, **240**, 599-624.
51 D. Primc, M. Drofenik and D. Makovec, *European J. Inorg. Chem.* 2011, **2011**, 3802−3809.
52 J. M. D. Coey, *IEEE Trans. Mag.* 2011, **47**, 4671-4681.
53 D. Lisjak and S. Ovtar, *J. Phys. Chem. B* 2013, **117**, 1644−1650.
54 S. Ovtar, D. Lisjak and M. Drofenik, *J. Am. Ceram. Soc.* 2011 **94**, 3373–3379.